Carbohydrate Polymers
May 2022, Volume 284 Pages 119191 (11p.)
https://doi.org/10.1016/j.carbpol.2022.119191
https://archimer.ifremer.fr/doc/00750/86163/

Microgels based on Infernan, a glycosaminoglycan-mimetic bacterial exopolysaccharide, as BMP-2 delivery systems

Gélébart Perrine [1], Cuenot Stéphane [2], Sinquin Corinne [1], Halgand Boris [3], Sourice Sophie [3, 4], Le Visage Catherine [3, 4], Guicheux Jérôme [3, 4, 5], Colliec-Jouault Sylvia [1], Zykwinska Agata [1, *]

[1] Ifremer, MASAE, 44300 Nantes, France
[2] Nantes Université, CNRS, Institut des Matériaux Jean Rouxel, IMN, Nantes, France
[3] Inserm, UMR 1229, RMeS, Regenerative Medicine and Skeleton, Université de Nantes, ONIRIS, F-44042 Nantes, France
[4] UFR Odontologie, Université de Nantes, Nantes, France
[5] CHU Nantes, PHU4 OTONN, Nantes, France

* Corresponding author : Agata Zykwinska, email address : Agata.Zykwinska@ifremer.fr

Abstract :

Bone Morphogenetic Protein (BMP-2) is an osteoinductive growth factor clinically used for bone regeneration. Tuneable sustained strategies for BMP-2 delivery are intensely developed to avoid severe complications related to supraphysiological doses applied. To address this issue, we investigated the ability of the bacterial exopolysaccharide (EPS) called Infernan produced by the deep-sea hydrothermal vent bacterium Alteromonas infernus, exhibiting both glycosaminoglycan-mimetic and physical gelling properties, to efficiently bind and release the bioactive BMP-2. Two delivery systems were designed based on BMP-2 retention in either single or complex EPS-based microgels, both manufactured using a microfluidic approach. BMP-2 release kinetics were highly influenced by the ionic strength, affecting both microgel stability and growth factor/EPS binding, appearing essential for BMP-2 bioactivity. The osteogenic activity of human bone-marrow derived mesenchymal stem cells studied in vitro emphasized that Infernan microgels constitute a promising platform for BMP-2 delivery for further in vivo bone repair.

Graphical abstract

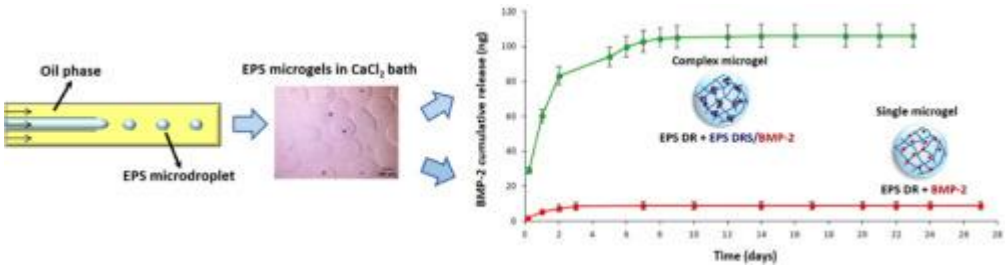

Keywords : Heparin-mimetic, Capillary microfluidics, Release kinetics, BMP-2 bioactivity, Osteogenic potential, AFM imaging

1. Introduction

Bone Morphogenetic Proteins (BMPs), belonging to the Transforming Growth Factor-β (TGF-β) superfamily, by inducing cellular processes, such as migration, proliferation, differentiation and adhesion play pivotal roles in the morphogenesis of a variety of tissues and organs (Ebara, 2002; Hogan, 1996). In particular, BMP-2 was shown to be one of the most powerful osteoinductive factor for bone regeneration (Gautschi, Frey, & Zellweger, 2007; Kusumoto *et al*., 1998; Okubo, Bessho, Fujimura, Iizuka, & Miyatake, 2000). BMP-2 actively contributes to the recruitment, proliferation and differentiation of osteoprogenitor cells during the bone healing process and its amount increases immediately after bone trauma (Caetano-Lopes *et al*., 2011; Zhao *et al*., 2006). In clinics, to achieve an efficient treatment, supraphysiological doses of BMP-2 are applied to overcome the short half-life of the protein due to its rapid proteolytic degradation (Poynton & Lane, 2002). An excessive dosage of BMP-2 is however associated with important side effects such as tissue oedema, inflammation and heterotopic ossification (Neovius, Lemberger, Docherty Skogh, Hilborn, & Engstrand, 2013; Shields *et al*., 2006). To overcome these drawbacks, materials with the ability to strongly, but reversibly bind BMP-2 are developed to allow the growth factor sustained release and its localized presentation, which remain crucial for efficient bone repair over long periods of time (Hettiaratchi, Miller, Temenoff, Guldberg, & McDevitt, 2014; Hettiaratchi *et al*., 2020; Kisiel *et al*., 2013; Krishnan *et al*., 2017). Since in the natural extracellular matrix, glycosaminoglycans (GAG), negatively charged polysaccharides, are involved in essential cellular processes through growth factor binding (Gandhi & Mancera, 2008; Miller, Goude, McDevitt, & Temenoff, 2014), delivery systems based on GAG have become particularly attractive (Caballero Aguilar, Silva, & Moulton, 2019; Subbiah & Guldberg, 2019). Due to its high BMP-2 affinity resulting from its high sulfate content, heparin was shown to enhance the growth factor osteogenic activity by sequestrating BMP-2 on the cell surface and mediating its

internalization (Jeon *et al*., 2008; Takada *et al*., 2003; Zhao *et al*., 2006). Heparin can reduce the amount of BMP-2 bound to cell layer or its receptors and maintain BMP-2 in culture medium, prolonging its biological activity (Takada *et al*., 2003). Heparin was either incorporated into bulk hydrogels based on hyaluronic acid to improve BMP-2 loading and release (Bhakta *et al*., 2013; Kisiel *et al*., 2013) or structured into microparticles, which are well adapted for growth factor loading due to their high surface area-to-volume ratio (Hettiaratchi *et al*., 2014; Hettiaratchi *et al*., 2020; Tellier, Miller, McDevitt, & Temenoff, 2015). Despite several advantages of using heparin, its anti-coagulant properties may induce adverse bleeding complications and its long-term administration can lead to the reduction of bone density and the development of osteoporosis (Wolinsky-Friedland, 1995; Muir *et al*., 1996). Moreover, its animal origin increases the risk of contamination by a non-conventional transmissible agent such as prions or emerging viruses due to a large "species-barrier" (DeAngelis, 2012).

Recently, a better understanding of the role of GAG has led to the development of GAG-mimetics, molecules displaying GAG structural and functional properties (Badri, Williams, Linhardt, & Koffas, 2018). Different classes of GAG-mimetics have been developed mainly based on natural polymers, especially, polysaccharides obtained from different sources, such as plant, algae, animals and microorganisms. Amongst microorganisms, bacteria can synthesize extracellular soluble polysaccharides such as exopolysaccharides (EPS), endowed with both unusual structures and diverse biological functions (Delbarre-Ladrat, Sinquin, Lebellenger, Zykwinska, & Colliec-Jouault, 2014). The use of EPS producing bacteria is highly advantageous over traditional sources used for polysaccharide output: (*i*) EPS production in bioreactors can be controlled and optimized to obtain high yields, (*ii*) polysaccharide is produced by bacteria directly into culture medium, any chemical extraction step is necessary to recover it (in contrast to GAG from animal origin), (*iii*) fermentation process allows a renewable EPS production with no risks due to raw material supply, and both composition and

structure of the final polymer are conserved. GAG-mimetics derived from EPS produced by deep-sea hydrothermal vent bacteria display biological activities similar to GAG, especially when they present acidic sugars and sulfate groups (Delbarre-Ladrat *et al*., 2014; Zykwinska *et al*., 2019a). *Alteromonas infernus* is a deep-sea hydrothermal vent bacterium producing a naturally slightly sulfated high-molecular weight EPS, called Infernan (GY785 EPS) (Raguénès *et al*., 1997; Roger, Kervarec, Ratiskol, Colliec-Jouault, & Chevolot, 2004; Makshakova, Zykwinska, Cuenot, Colliec-Jouault, & Perez, 2022). In our previous studies, GAG-mimetic activities, including chondrogenic potential, anticoagulant and antimetastatic properties of the native EPS or its highly sulfated low-molecular weight derivatives, EPS DRS_{LMW} (20,000 – 30,000 g/mol and 12 - 14 wt% S) were shown both *in vitro* and *in vivo* (Merceron *et al*., 2012; Heymann *et al*., 2016; Rederstorff *et al*., 2017; Colliec-Jouault *et al*., 2001). For cartilage engineering purposes, the presence of heparin-mimetic EPS DRS_{LMW} was shown to stimulate the *in vitro* chondrogenic differentiation of human adipose-derived mesenchymal stem cells, through its physical interaction with Transforming Growth Factor-β1 (TGF-β1) (Merceron *et al*., 2012). In these previous studies, Infernan and its derivatives were used in their soluble form. However, we have recently shown that the EPS anionic nature confers to the EPS not only its GAG-mimetic properties, *i.e.* growth factor binding ability but also its capacity to form physical gel with divalent cations, such as calcium (Zykwinska *et al*., 2019b; Makshakova *et al*., 2022). This GAG-mimetic EPS was thus structured into bioactive physical microgels for TGF-β1 delivery using capillary microfluidics. Only few studies deal with a growth factor loading within polysaccharide-based microgels using a microfluidic approach (Moshaverinia, Xu, Chen, Akiyama, Snead, & Shi, 2013; Zykwinska *et al*., 2019b). However, this technique presents several advantages over other emulsification techniques, amongst homogenization and ultrasonication. It allows the formation of monodisperse microdroplets of controlled size, without using high energy and temperature conditions (Zhang, Tumarkin, Sullan, Walker, &

106 Kumacheva, 2007; Marquis, Davy, Cathala, Fang, & Renard, 2015; Zykwinska *et al*., 2016).
107 Microdroplets are solidified to form gelled microparticles or microgels by chemical,
108 photochemical or physical methods directly into the microfluidic device or in the collecting
109 bath. Contrary to other emulsification techniques, where the encapsulation of active
110 compounds, such as growth factors, is ensured by their adsorption inside microdroplets through
111 their diffusion from solution (Hettiaratchi *et al*., 2014; Hettiaratchi *et al*., 2020; Tellier *et al*.,
112 2015), microfluidic offers a unique possibility to formulate microdroplets and encapsulate the
113 totality of the active compound in only one step process.

114 In this context, the objective of the present study was to further exploit physico-chemical
115 (gelling) and biological (GAG-mimetic) properties of Infernan and its derivatives to develop
116 EPS-based microgels appropriate for bone healing purposes. Although the chondrogenic
117 potential of Infernan and its derivatives was clearly shown in our previous studies, their
118 osteogenic activity was not completely explored. However, this point remains crucial for further
119 development of efficient treatment for subchondral bone repair. To better understand the impact
120 of the polysaccharide sulfate content on the growth factor binding and release kinetics, BMP-2
121 was either directly loaded into microgels based on a slightly sulfated medium-molecular weight
122 EPS derivative (EPS DR_{MMW}) or firstly complexed with highly sulfated low-molecular weight
123 derivative (EPS DRS_{LMW}), exhibiting heparin-mimetic properties, prior to its loading into EPS
124 DR_{MMW} microgels (Figure 1). Both microgels were generated using a capillary microfluidic
125 approach. BMP-2 release from single (EPS DR_{MMW} + BMP-2) and complex (EPS DR_{MMW} +
126 EPS DRS_{LMW}/BMP-2) microgels was then assessed in media with different ionic strengths.
127 Bioactivity of growth factor released from microgels was then evaluated by stimulating murine
128 osteoblastic MC3T3-E1 cells. Finally, the effect of BMP-2 released from complex microgels
129 on the *in vitro* osteogenic activity of human bone-marrow derived mesenchymal stem cells
130 (hBM-MSC) was assessed by measuring the alkaline phosphatase (ALP) activity and matrix

mineralization ability. The main hypothesis of this study was related to the ability of Infernan-based microgels to efficiently bind and then release bioactive BMP-2 that can further induce expected cellular responses.

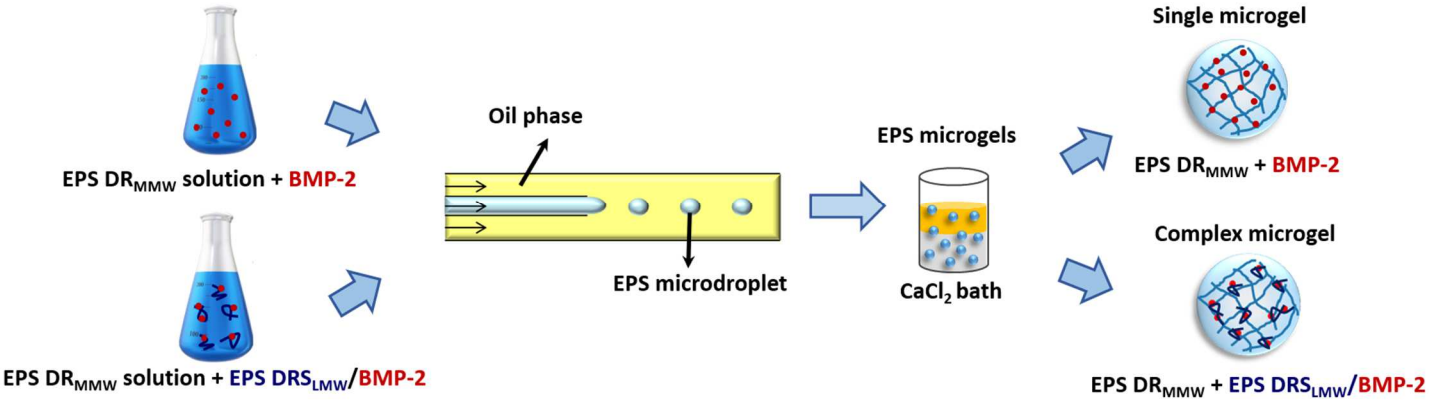

Figure 1. (A) Schematic representation of preparation of BMP-2 loaded single (EPS DR_{MMW} + BMP-2) and complex (EPS DR_{MMW} + EPS DRS_{LMW}/BMP-2) microgels based on Infernan (GY785 EPS) by capillary microfluidic approach.

2. Materials and Methods

2.1. Production of the native Infernan (GY785 EPS) by *A. infernus* fermentation

The production of the EPS was previously described (Raguénès *et al.*, 1997). Briefly, *A. infernus* was cultured at 25°C in Zobell medium composed of yeast extract (1 g/L), tryptone (4 g/L) and aquarium salts (33.3 g/L) at pH 7.4 in a 30 L fermenter (Techfors 30 L INFORS, Switzerland). Glucose at 30 g/L was added as a carbon source. After 48 h of fermentation, the culture medium was centrifuged at 9000 g for 45 min, the supernatant containing soluble EPS was ultrafiltrated on a 100 kDa cut-off membrane and freeze-dried.

2.2. Preparation of EPS derivatives, EPS DR and EPS DRS, and their physico-chemical characterizations.

EPS derivatives were prepared, as previously described (Chopin *et al*., 2015). Briefly, the native EPS (2.5 g) solubilized in water (350 mL) was depolymerized at 60°C for 45 min using hydrogen peroxide added dropwise. After overnight reduction by sodium borohydride and purification on Chelex® 20 resin, the solution containing depolymerized EPS (EPS DR) was ultrafiltrated on a 10 kDa cut-off membrane and freeze-dried. To obtain homogeneous fractions of EPS DR with low polydispersity, a predominant population of polysaccharide chains with a narrow molecular weight distribution was selected by a gel filtration chromatography on either Superdex® 30 (EPS DR_{LMW} of 20,000 g/mol) or Sephacryl S-100 HR (EPS DR_{MMW} of 260,000 g/mol) (Cytiva), using an AKTA FPLC system coupled with a refractometric detector (Hitachi L2490). Samples eluted with water were pooled and freeze-dried.

Highly sulfated low-molecular weight derivative (EPS DRS_{LMW}) was obtained by a chemical oversulfation of EPS DR_{LMW} of 20,000 g/mol, as descried earlier (Zykwinska *et al*., 2019b; Chopin *et al*., 2015). Briefly, EPS DR_{LMW} (50 mg) in its pyridinium salt form was firstly solubilized in anhydrous DMF (100 mL) at 45°C for 2 h under continuous stirring and then sulfated for the next 2 h at 45°C in the presence of SO_3.Py (250 mg). The final aqueous solution (pH 7) was dialyzed against water for three days prior to be freeze-dried.

Monosaccharide composition of the native EPS and EPS DR was determined according to Kamerling *et al*. (1975) method, modified by Montreuil *et al*. (1986). EPS DRS_{LMW} could not be analyzed properly due to its high sulfate content, which prevents from correct derivatization and formation of the per-O-trimethylsilyl methyl glycosides. Briefly, samples were hydrolyzed using MeOH/HCl at 100°C for 4 h. Myo-inositol was used as internal standard. The methyl glycosides thus obtained were then converted to trimethylsilyl derivatives using *N*,*O*-bis(trimethylsilyl)trifluoroacetamide and trimethylchlorosilane (BSTFA:TMCS) 99:1. Gas

chromatography (GC-FID, Agilent Technologies 6890N) was used for separation and quantification of the per-O-trimethylsilyl methyl glycosides formed.

Weight-average molecular weight of the native EPS and its derivatives (EPS DR and EPS DRS) was determined by High-Performance Size-Exclusion Chromatography (HPSEC, Prominence Shimadzu) coupled with a multiangle light scattering (MALS, Dawn Heleos-II, Wyatt Technology) and a differential refractive index (RI) (Optilab Wyatt technology) detectors. Samples were eluted with 0.1 M ammonium acetate. The molecular weight was calculated using a refractive index increment dn/dc of 0.145 used for polysaccharides.

The linked ester sulfate group content of the native EPS and its derivatives (EPS DR and EPS DRS) was determined using High-Performance Anion-Exchange Chromatography (HPAEC) (Dionex DX-500) by calculating the difference between the total sulfur content in the hydrolyzed sample and in the non-treated sample (free sulfur), as previously described by Chopin *et al*. (2015).

2.3. Single and complex microgel formation using capillary microfluidics

Single microgels (EPS DR_{MMW} + BMP-2) were prepared by mixing 1.5 mL of EPS DR_{MMW} (260,000 g/mol) aqueous solution (final concentration of 30 mg/mL) with 500 µL of recombinant human BMP-2 (CHOcells, PeproTech, Neuilly-sur-Seine, France) at 34 µg/mL in water. To prepare complex microgels (EPS DR_{MMW} + EPS DRS_{LMW}/BMP-2), 500 µL of EPS DRS_{LMW} (31,000 g/mol) aqueous solution at 3.4 mg/mL was mixed with 500 µL of BMP-2 at 34 µg/mL in water and incubated for 1 h at 37°C under gentle stirring. EPS DRS_{LMW}/BMP-2 complex solution was then added to 1 mL of EPS DR_{MMW} aqueous solution at the final concentration of 30 mg/mL. To structure EPS DR_{MMW} into microgels, a home-made capillary microfluidic co-flow device was developed. The dispersed phase containing either EPS DR_{MMW} + BMP-2 or EPS DR_{MMW} + EPS DRS_{LMW}/BMP-2 aqueous solution was delivered through a silica tube with interior diameter of 75 µm inserted into chromatography tee fitting. The

continuous phase, a sunflower seed oil (Fluka), was delivered through a Fluorinated Ethylene Propylene (FEP) 1/16" tube (ID 750 µm, OD 1.57 mm) (Cluzeau Info Labo, France) perpendicularly to the tee fitting. The dispersed phase co-flowed in a FEP 1/16" tube (ID 750 µm, OD 1.57 mm) containing the continuous oil phase. The following flow rates were applied to produce microdroplets: dispersed phase at 2 µL/min and continuous phase at 120 µL/min. The flow rates were controlled using Microfluidic Flow Control System MFCS^{TM}-EZ with flow-rate platform (Fluigent). The device was run for 30 min per sample, allowing to prepare single and complex microgels with the final concentrations of BMP-2 and EPS DRS_{LMW} of around 500 ng/mL and 50 µg/mL (in 1 mL), respectively. Microgels were recovered in collecting bath containing 10 mL of 360 mM $CaCl_2$. After overnight storage at 4°C, microgel suspensions were washed three times with either 2 mM or 180 mM $CaCl_2$ aqueous solutions prior to release experiments started immediately after washing step.

2.4. *In vitro* BMP-2 release from microgels and stability assessment of microgels

In vitro release study was performed in three different conditions: Dulbecco's Modified Eagle Medium (DMEM, ThermoFisher Scientific), 2 mM and 180 mM $CaCl_2$ aqueous solutions at 37°C. Firstly, BMP-2 release was performed in DMEM containing Bovine Serum Albumin (BSA) at 1%. Single and complex microgel suspensions after washing step in 2 mM $CaCl_2$ were either directly incubated in DMEM/BSA 1% (non-equilibrated microgels) or firstly equilibrated in 1 mL of 2 mM $CaCl_2$ for another 24h at 4°C and then incubated in 1 mL of DMEM/BSA 1% (equilibrated microgels). For the release study in $CaCl_2$ solutions, single and complex microgels were either directly incubated in 1 mL of 180 mM $CaCl_2$/BSA 1% after washing step in the same solution or firstly equilibrated in 1 mL of 2 mM $CaCl_2$ for 24h at 4°C followed by the release experiment in 1 mL of 2 mM $CaCl_2$/BSA 1%. All samples were incubated at 37°C under continuous shaking for 23 or 27 days. At different incubation times, 500 µL of the supernatant were removed after centrifugation step (5 min, 2000 g) and replaced by a fresh buffer (500 µL).

Release experiments were performed in duplicate for each condition and each time from two independent encapsulation experiments. The recovered supernatants were stored at -20°C prior to analyses. The amount of BMP-2 released from microgels during (*i*) the overnight storage in 360 mM $CaCl_2$ at 4°C, (*ii*) the equilibration step in 2 mM $CaCl_2$ for 24h at 4°C and (*iii*) the release experiments run for 23 or 27 days at 37°C was determined using ELISA Duoset® assay kit (DY355, R&D Systems – Bio-Techne). The standard curves were obtained in an appropriate buffer, 2 mM $CaCl_2$, 180 mM $CaCl_2$ or DMEM. In addition, the standard curves using BMP-2 mixed with EPS DRS_{LMW} at 1, 5 and 50 µg/mL in DMEM were prepared.

In parallel to the release experiments, the stability of microgels was assessed in each condition tested by measuring the microgel size every day using an optical microscope (Optika, Italy). Scanning Electron Microscopy (SEM) observations on freeze-dried microgels were performed using JEOL 7600F instrument (JEOL, US).

2.5. Surface Plasmon Resonance (SPR).

SPR experiments were carried out on a Biacore 3000 instrument (Cytiva). BMP-2 (CHOcells, PeproTech, Neuilly-sur-Seine, France) was covalently immobilized to the dextran matrix of a CM5 sensor chip (Biacore), as recommended by the manufacturer at a flow rate of 5 µL/min. Binding assays of EPS DR_{LMW} (20,000 g/mol), EPS DRS_{LMW} (31,000 g/mol) and heparin (15,000 g/mol, H4784 Sigma) were performed in 10 mM HEPES at pH 7.4 containing 150 mM NaCl and 0.005% P2O surfactant (HBS-P buffer,Biacore) with dissociation monitored for 15 min. Regeneration was achieved with NaOH (4.5 mM/L) after each cycle. The resulting sensorgrams were fitted using BiaEval 4.1 software (Biacore).

2.6. Atomic Force Microscopy (AFM) imaging.

For AFM imaging, BMP-2 was prepared at 5 µg/mL in water. Solutions of EPS DRS_{LMW}/BMP-2 complexes and of EPS DR_{MMW} containing EPS DRS_{LMW}/BMP-2 complexes prepared for microfluidic encapsulation were observed after 5-fold and 200-fold dilution in water, respectively. Five µL of each solution were deposited onto freshly cleaved mica surface and dried at 20°C. AFM images were recorded using a NanoWizard® Atomic Force Microscope (JPK, Germany) in intermittent contact mode in air at room temperature. A standard rectangular cantilever (Nanosensors NCL-W) with a free resonance frequency of 170 kHz and a spring constant of 40 N/m was used. AFM tip with a radius curvature of ~5 nm was cleaned by UV-ozone treatment prior to AFM observations. Each sample was imaged on three different zones. JPK Data Processing software (JPK, Germany) was used for image processing and height measurements (N = 50 per sample).

2.7. Size distribution of BMP-2, EPS DRS and EPS DRS/BMP-2 complexes by dynamic light scattering (DLS) measurements

A Zetasizer Nano Series (Malvern Instrument, UK) was used to determine the hydrodynamic diameter of soluble BMP-2 (500 ng/mL), soluble EPS DRS_{LMW} (50 µg/mL) and EPS DRS_{LMW}/BMP-2 complexes, as prepared for microfluidic encapsulation. Additionally to the control samples, the supernatants recovered during the incubation of complex microgels in either 2 mM or 180 mM $CaCl_2$ for 48h were analyzed. Solutions were analyzed at 20°C in a backscattering configuration at 173° for 120 s. The hydrodynamic diameter was measured in triplicate for each sample. A refractive index of 0.145 was used to determine the volume-size distribution.

2.8. BMP-2 bioactivity assay.

Bioactivity of BMP-2 released from microgels was assessed by measuring activation of Smads 1,5,8 signaling pathway after stimulation of murine MC3T3-E1 Subclone 4 (CRL-2593™ from ATCC) with the supernatants from release experiments, as described previously (Guicheux *et al*., 2003). MC3T3-E1 cells were cultured in α-MEM supplemented with 10% Fetal Bovine Serum (FBS, Dominique Dutscher) and 1% glutamine and 1% Penicillin/Streptomycin (P/S, Thermo Fisher Scientific) at 37°C and 5% CO_2. Cells were seeded on six-well plates at 40,000 cells/cm^2 and proliferated until reaching 80% confluence. To synchronize the cells, the medium was changed to 0.5% FBS 12h before stimulation.

MC3T3-E1 were stimulated with the supernatants containing BMP-2 released from complex microgels (EPS DR_{MMW} + EPS DRS_{LMW}/BMP-2) in DMEM or in 2 mM $CaCl_2$. Soluble BMP-2 (sBMP-2) (100 ng/mL), soluble EPS DRS_{LMW} (50 µg/mL) and EPS DRS_{LMW}/BMP-2 complex (final concentration of 50 µg/mL EPS DRS_{LMW} and 500 ng/mL BMP-2) were used as controls. Release supernatants recovered at different time points: day D0 (4h or 5 h), D1, D2, D5, D7, D14, D21 were incubated with MC3T3-E1 for 1 h at 37°C. Medium was then removed and cells were snapped freezed in liquid nitrogen. Proteins were then extracted on ice using homemade RIPA buffer and assayed with the Pierce BCA™ Protein Assay Kit (23225, Thermo Fisher Scientific). For Western Blot experiments, after migration on AnykD Criterion™ Midi TGX™ Stain-Free precast gels (Bio-Rad), proteins were transferred onto Trans-Blot Turbo Midi PVDF transfer Packs (Bio-Rad) using the Transblot® Turbo™ Transfer System (Bio-Rad). Total Smad 1 and Phosphorylated-Smad 1,5,8 were analyzed using specific antibodies for cells stimulated with BMP-2, as described previously (Guicheux *et al*., 2003). All primary antibodies were revealed by an anti-rabbit secondary antibody (Cell Signalling) and the SuperSignal™West Dura substrate for Smad 1 or Femto substrate for Phosphorylated-Smad 1,5,8 (ThermoFisher Scientific) using the ChemiDoc™ MP Imaging System (Bio-Rad) and the

Image Lab software. Bioactivity assay was performed in duplicate using equilibrated complex microgels from two encapsulation experiments.

2.9. Effect of BMP-2 released from complex microgels on the *in vitro* osteogenic activity of hBM-MSC.

The *in vitro* osteogenic activity of hBM-MSC (451Z012.1 from PromoCell) in the presence or absence of BMP-2 released from equilibrated complex microgels was studied by measuring ALP activity and Alizarin red staining. hBM-MSC cells were seeded on 24-well plates at 10,000 cells per cm² in 500 µL of DMEM supplemented with 10% FBS and 1% Penicillin/Streptomycin (P/S, ThermoFisher Scientific) at 37°C and 5% CO_2. After 24h, medium was switched to osteogenic differentiation medium (ODM) composed of DMEM supplemented with 10% FBS, 1% P/S, 10 mM β-glycerophosphate, 50 µM ascorbic acid and dexamethasone. Control medium was composed of DMEM supplemented with 10% FBS and 1% P/S. Suspension of equilibrated complex microgels loaded with BMP-2 (EPS DR_{MMW} + EPS DRS_{LMW}/BMP-2) was deposited (200 µL in DMEM) on Transwell inserts with an 8 µm pore polycarbonate membrane (Corning, 3422, Kennebunk ME, USA) placed above 24-well plate with hBM-MSC. In parallel, unloaded complex microgels (EPS DR_{MMW} + EPS DRS_{LMW}), unloaded complex microgels supplemented with soluble BMP-2 (100 ng/mL) (EPS DR_{MMW} + EPS DRS_{LMW} + sBMP-2), soluble BMP-2 (100 ng/mL) and DMEM were used as controls. Transwell experiments (two independent experiments performed in duplicate) were carried out for either 7 or 16 days in ODM changed every three days. Soluble sBMP-2 was supplemented every three days. ALP activity of hBM-MSC stimulated by BMP-2 from transwell experiments was measured according to the Bessey-Lowry enzymological method (Bessey, Lowry, & Brock, 1942). Cells were washed twice with PBS and then dry frozen at -80°C. ALP activity in cell lysate was measured by Alkaline Phosphatase Substrate kit (Biorad 172-1063) using p-

nitrophenyl phosphate (pNPP). ALP activity was normalized by a total protein content determined using the Pierce BCA™ Protein Assay Kit (23225, Thermo Fisher Scientific). Alizarin red staining was performed after 16 days of culture, as described by Lavenus *et al*. (2011). As before, the mineralization was determined in both standard and osteogenic media. The culture medium was discarded, confluent cell layers were washed with PBS and staining with alizarin red S (2%, pH 4.2, Merck) was performed for 2 min. After aspiration of the overflow, cells were washed three times with water. Staining layers were visualized by optical microscopy (Nikon Instruments Inc.).

3. Results and discussion

3.1. Native EPS and its derivatives.

Native EPS synthesized by *A. infernus* is a naturally slightly sulfated highly branched anionic heteropolysaccharide with a complex repeating unit composed of nine osidic residues (Raguénès *et al*., 1997; Roger *et al*., 2004). Its main chain is composed of glucose (Glc), galacturonic acid (GalA) and galactose (Gal), covalently linked in the sequence: →4)-β-D-Glcp-(1→4)-α-D-GalpA-(1→4)-α-D-Galp-(1→. GalA residue is substituted at O-2 by one sulfate group and at O-3 by a short side chain constituted of two glucuronic acids (GlcA), Gal and Glc linked in the sequence: β-D-Glcp-(1→6)-α-D-Galp-(1→4)-β-D-GlcpA-(1→4)-β-D-GlcpA-(1→. In addition, the two GlcA of the side chain are each substituted by a terminal Glc (Roger *et al*., 2004). The presence of three consecutive uronic acids per repeating unit and one sulfate group confers to Infernan its gelling properties in the presence of divalent cations, such as calcium (Zykwinska *et al*., 2019b; Makshakova *et al*., 2022). It was previously shown that by decreasing the molecular weight of the native EPS (~2,000,000 g/mol) to intermediate molecular weight derivatives, physical gelation with calcium ions was favoured. Herein, slightly sulfated medium-molecular weight EPS DR_{MMW} of ~260,000 g/mol was prepared by a

free-radical depolymerization of the native EPS. The depolymerization reaction had no major impact on the polysaccharide structure (Table 1). Besides decreasing the molecular weight, the depolymerization process was previously shown to efficiently decrease the amount of the lipopolysaccharides (LPS) present within the EPS produced by *A. infernus*, being a Gram-negative bacterium (Grivaud-Le Du *et al*., 2017). Indeed, the endotoxin level decreased from 72,500 EU/mg for the native high molecular weight EPS to 135 EU/mg for the low-molecular weight derivative of 30,000 g/mol. Biochemical and chemical analyses of the LPS extracted from *A. infernus* membranes have shown the lack of the typical LPS architecture (absence of 3-deoxy-D-manno-oct-2-ulopyranosonic acid (Kdo), glucosamine (GlcN), and phosphorylated monosaccharides), such as that known for *Escherichia coli* (Grivaud-Le Du *et al*., 2017). This suggests that the outer membrane of *A. infernus* is most likely composed of peculiar glycolipids, which did not induce toxic effects, as previously observed in our *in vivo* studies (Heymann *et al*., 2016; Rederstorff *et al*., 2017).

Table 1. Monosaccharide composition (wt%), sulfur content (wt%) and weight average molecular weight, Mw (g/mol) of the native slightly sulfated high-molecular weight EPS, slightly sulfated medium molecular weight derivative, EPS DR_{MMW}, slightly sulfated low-molecular weight derivative, EPS DR_{LMW} and highly sulfated low-molecular weight derivative, EPS DRS_{LMW}.

	Monosaccharide composition (wt%)							**S (wt%)**	**Mw (g/mol)**
	Rha	**Fuc**	**Man**	**Gal**	**Glc**	**GlcA**	**GalA**		
Native EPS	2.2	1.5	4.2	10.4	18.5	12.7	7.6	3.2	2,000,000
EPS DR_{MMW}	1.1	0.7	2.5	8.8	12.8	15.7	9.2	3.2	260,000
EPS DR_{LMW}	0	0	0	12.2	11.9	9.8	7.3	3.3	20,000
EPS DRS_{LMW}	nd	nd	nd	nd	nd	nd	nd	14.0	31,000

Rha: rhamnose, Fuc: fucose, Man: mannose, Gal: galactose, Glc: glucose, GlcA: glucuronic acid, GalA: galacturonic acid.
nd: non-determined

3.2. Single and complex microgel formation by capillary microfluidics.

In the following step, EPS DR_{MMW} was formulated in BMP-2 loaded microgels using a home-made capillary microfluidic co-flow device (Figure 1). To obtain single microgels (EPS DR_{MMW} + BMP-2), BMP-2 was directly solubilized in EPS DR_{MMW} aqueous solution and formulated into microgels. In the case of complex microgels (EPS DR_{MMW} + EPS DRS_{LMW}/BMP-2), BMP-2 was firstly incubated for 1h at 37°C with highly sulfated low-molecular weight derivative, EPS DRS_{LMW} (31,000 g/mol and 14 wt% S) obtained after oversulfation of low-molecular weight derivative, EPS DR_{LMW} (20,000 g/mol and 3.3 wt% S) (Table 1). EPS DRS_{LMW}/BMP-2 complex was then incorporated within EPS DR_{MMW} aqueous solution, which was further structured in complex microgels. Single and complex microgels with similar sizes of 463 µm ± 63 µm in diameter were collected in 360 mM $CaCl_2$ bath by applying the same experimental conditions (the same flows of disperse and continuous phases) (Figure 2A). No major differences in morphologies were noticed between single and complex microgels, as revealed by SEM (Figure 2B). In both cases, a porous structure was clearly observed.

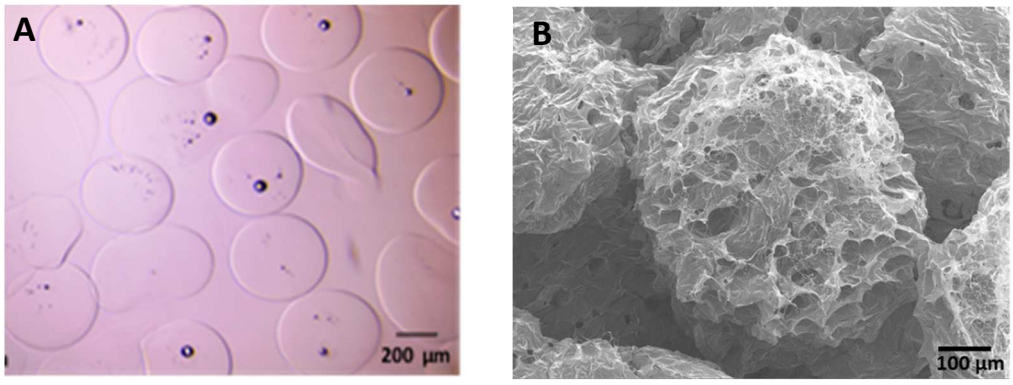

Figure 2. (A) Optical microcopy image of complex microgels collected in 360 mM $CaCl_2$ bath. (B) SEM image of freeze-dried complex microgels.

The complexation of positively charged BMP-2 (pI ~9) with negatively charged EPS DRS_{LMW} before growth factor loading inside microgels may further preserve the growth factor from degradation and improve its half-life and bioactivity. SPR analyses revealed very high binding

affinity of BMP-2 for EPS DRS_{LMW} with dissociation constant *Kd* of 0.63 nM, compared to that obtained for EPS DR_{LMW} with *Kd* of 0.1 µM. Growth factor affinity for EPS DRS_{LMW} was even higher than for unfractionated heparin (15,000 g/mol) with *Kd* of 8.29 nM for similar sulfur content (12-14 wt% S). To reveal the ability of EPS DRS_{LMW} to bind BMP-2 and to form assemblies, AFM imaging was used (Figure 3). Free BMP-2 in water was compared to BMP-2 mixed with EPS DRS_{LMW} (EPS DRS_{LMW}/BMP-2 complex) and to EPS DRS_{LMW}/BMP-2 complex incorporated in EPS DR_{MMW} solution, as used for microfluidic encapsulation. Figure 3A shows BMP-2 nanoparticles with diameters varying from 2 to 10 nm (height measurements), which are consistent with the size of the protein homodimer of 70 Å x 35 Å x 30 Å, the biologically active form (Scheufler, Sebald, & Hülsmeyer, 1999). When BMP-2 was mixed with the highly-sulfated EPS derivative to prepare EPS DRS_{LMW}/BMP-2 complexes for microfluidic encapsulation, only larger nanoparticles of 10 nm to 30 nm in diameter were observed, indicating the absence of free BMP-2 (Figure 3B). It appeared that upon incubation, positively charged BMP-2 co-assembled with negatively charged EPS DRS_{LMW}, leading to nanoparticles of higher diameters. Incorporation of these complexes into EPS DR_{MMW} solution prior to microfluidic encapsulation, caused further nanoparticle assembly, since an increase in measured diameters was noted. Indeed, the nanoparticle assembly diameters varied from 15 nm to 60 nm (Figure 3C). The ability to form nanoassemblies between BMP-2 and EPS DRS_{LMW} may have a considerable impact on both growth factor bioactivity and biodisponibility. In our previous study, only highly sulfated EPS derivative was shown to stimulate *in vitro* hATSC chondrogenic differentiation in the presence of TGF-β1, probably through electrostatic interactions with the growth factor (Merceron *et al*., 2012). Non-covalent binding of TGF-β1 to EPS DRS_{LMW} enhanced the growth factor bioactivity, in comparison to a slightly sulfated EPS DR_{LMW} (Merceron *et al*., 2012; Zykwinska *et al*., 2019b). It was shown by AFM that the

positively charged TGF-β1 also formed nanoassemblies with the negatively charged EPS DRS_{LMW} (Zykwinska *et al.*, 2018).

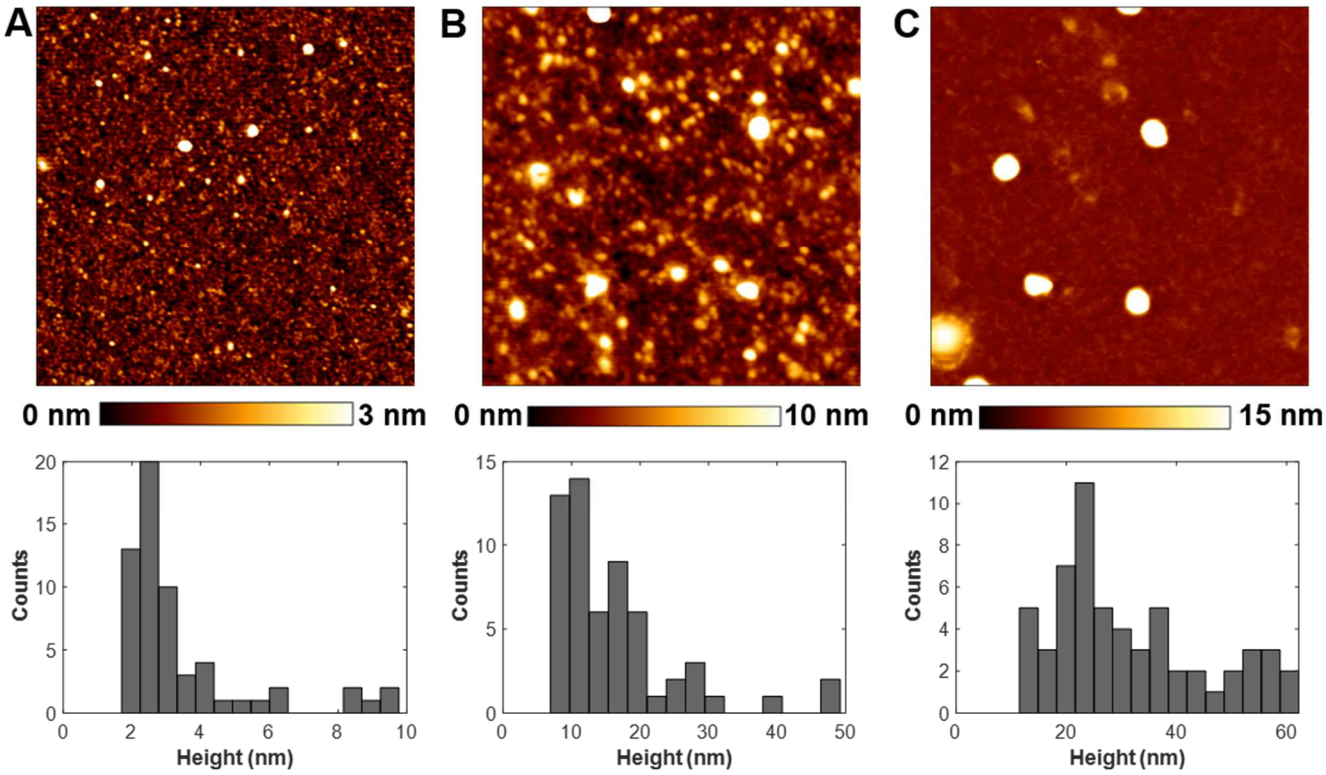

Figure 3. AFM height images (2 µm x 2 µm) and height distribution of (A) BMP-2, (B) EPS DRS_{LMW}/BMP-2 complexes and (C) EPS DR_{MMW} with EPS DRS_{LMW}/BMP-2 complexes. All sample solutions in water were dried on mica surface at 20°C prior to imaging in intermittent contact mode in air.

3.3. *In vitro* BMP-2 release from single and complex microgels.

BMP-2 release was firstly followed under *in vitro* conditions by incubating single or complex microgels in cell culture medium (DMEM). Since DMEM is particularly rich in inorganic salts, the effect of salt concentration on BMP-2 release from microgels was further assessed at two different ionic strengths, either at physiological calcium concentration in 2 mM $CaCl_2$ or at high ionic strength in 180 mM $CaCl_2$. Considering that the microfluidic approach allows to encapsulate the totality of BMP-2 during microdroplet formulation and by taking into account

425 the run time for the microgel production, the flow rate of the dispersed phase and the growth
426 factor concentration, it can be estimated that around 500 ng/mL of BMP-2 were encapsulated
427 within both single and complex microgels per tube used for each release experiment performed
428 in 1 mL. The amount of BMP-2 released from both single and complex microgels measured by
429 ELISA during their overnight storage in 360 mM $CaCl_2$ at 4°C as well as during their
430 equilibration in 2 mM $CaCl_2$ for 24h at 4°C was very low (< 2 ng/mL). The amount determined
431 was systematically added to each release experiment at day 0.
432
433 *3.3.1. BMP-2 release from single and complex microgels in DMEM.*
434 The profiles obtained for BMP-2 released from single and complex microgels upon incubation
435 in DMEM are presented on Figure 4A. Low growth factor release was observed from single
436 microgels (EPS DR_{MMW} + BMP-2), as only 8.4 ng of BMP-2 were quantified in the supernatant
437 after 3 days of incubation and no evolution was further observed. Weak growth factor binding
438 to single microgels may result in a rapid BMP-2 degradation leading to undetectable protein.
439 In contrast, different profiles were observed for BMP-2 loaded complex microgels, depending
440 if they were equilibrated in 2 mM $CaCl_2$ for 24 h before release in DMEM or not. Equilibrated
441 complex microgels exhibited fast growth factor release kinetic with a burst release of 29 ng of
442 BMP-2 for the first 5 h, followed by a rapid increase in growth factor concentration during the
443 first 2 days (27 ng of BMP-2 per day) up to 83 ng. Afterwards, the amount of growth factor
444 increased only slightly to reach 103 ng at 7 days with a rate of 4 ng per day. No increase in
445 BMP-2 released was further observed. In comparison, the release kinetic from non-equilibrated
446 complex microgels was considerably slower. Lower burst release of 11.5 ng of BMP-2 during
447 the first 4 h was firstly observed, followed by a sustained growth factor release up to 65.8 ng of
448 BMP-2 for 15 days with a rate of 3.6 ng per day. Then, slower release rate of 0.5 ng of BMP-2
449 per day was still observed to reach 72 ng of BMP-2 released during 27 days. Considering that

450 the initial amount of the growth factor encapsulated within microgels was of 500 ng/mL, the
451 total release of BMP-2 in equilibrated and non-equilibrated complex microgels was of 20.6%
452 and 14.4%, respectively.
453 Greater and faster BMP-2 diffusion from equilibrated complex microgels, observed especially
454 during the first hours, is due to the mechanical weakness of the physical microgel network,
455 resulting from the equilibration step. In this step, microgels collected in 360 mM $CaCl_2$ were
456 incubated in 2 mM $CaCl_2$ for 24h at 4°C to decrease the calcium concentration to a
457 physiological calcium concentration present in DMEM. During this ionic concentration change,
458 the density of cross-links between polysaccharide chains mediated by calcium ions decreased,
459 leading to a looser network compared to the initial network formed in 360 mM $CaCl_2$. At this
460 step, a weak swelling of ~15% was observed, as microgel diameter increased from 463 µm ±
461 63 µm to 535 µm ± 53 µm. As microgels swelled only weakly, the release of BMP-2 from the
462 microgels during this step was very low, as measured by ELISA assay (< 2 ng/mL). The
463 difference in the network cross-linking density between equilibrated and non-equilibrated
464 microgels clearly impacted the release profiles measured in DMEM at 37°C. Indeed, the
465 presence of inorganic salts (e.g. 110 mM sodium chloride) provoked a faster network loosening
466 resulting from calcium exchange in equilibrated microgels compared to non-equilibrated ones.
467 A rapid swelling of both complex microgels was observed within the first 24 h, where the
468 microgel diameter increased up to 719 ± 53 µm and 824 µm ± 85 µm for non-equilibrated and
469 equilibrated complex microgels, respectively. After 5 days of incubation in DMEM, mainly
470 microgel debris were observed.
471
472 *3.3.2. BMP-2 release from single and complex microgels at two ionic strengths.*
473 The effect of salt concentration on BMP-2 release from single and complex microgels was
474 further studied in $CaCl_2$ aqueous solutions at two different ionic strengths, either 2 mM or 180

475 mM (Figure 4B). At high ionic strength (180 mM $CaCl_2$), single microgels displayed only weak
476 BMP-2 release with a plateau value of 9 ng rapidly reached within the first 3 days, as already
477 observed in DMEM. It appeared once again that single microgels are not suitable for BMP-2
478 release. Indeed, slightly sulfated EPS DR_{MMW} used for microgel formation is unable to
479 efficiently protect BMP-2 from degradation. Similar results were reported for partially
480 desulfated heparin microparticles, where BMP-2 release was shown to be dependent on
481 sulfation pattern, with the lowest release of detectable growth factor observed from more
482 desulfated heparin microparticles (Tellier *et al.*, 2015). However, upon incubation of complex
483 microgels in 180 mM $CaCl_2$, a sustained release of BMP-2 was observed with the initial burst
484 release of 5.8 ng of BMP-2 for the first 4 h. Then, a progressive release of BMP-2 was observed
485 for 18 days, with the rate of 3.7 ng per day, to reach a plateau value of 73 ng of BMP-2 released.
486 The BMP-2 release kinetic at high ionic strength was very similar to that observed in DMEM
487 for non-equilibrated complex microgels with the total release of 14.6% of BMP-2 initially
488 loaded. Interestingly, when complex microgels were incubated at low ionic strength (2 mM
489 $CaCl_2$), very low growth factor release was observed, as only 3.8 ng of BMP-2 were quantified
490 in the supernatant for 23 days. During the release experiments performed in $CaCl_2$ solutions at
491 37°C, complex microgels progressively swelled to reach the diameters of 902 µm ± 82 µm and
492 723 µm ± 74 µm in 2 mM and 180 mM $CaCl_2$, respectively, at 14 days of incubation. Beyond
493 14 days, microgels started to dissolve. It was noted that in the case of $CaCl_2$ solutions, the
494 incubation at 37°C induced swelling and final dissolution of microgels, while they remained
495 almost unchanged during their storage at 4°C for one month.

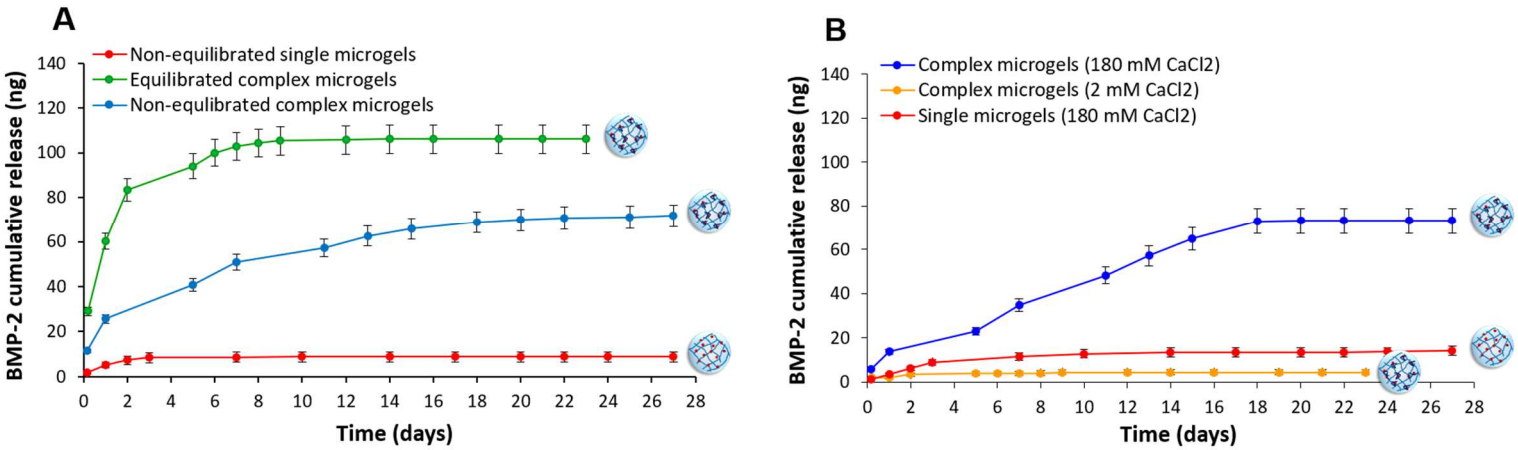

496

497 Figure 4. (A) BMP-2 cumulative release from non-equilibrated single microgels (EPS DR_{MMW} + BMP-
498 2), equilibrated (2 mM $CaCl_2$, 24h, 4°C) and non-equilibrated complex microgels (EPS DR_{MMW} + EPS
499 DRS_{LMW}/BMP-2) upon incubation in DMEM at 37°C for 23 or 27 days. (B) BMP-2 cumulative release
500 from single microgels (EPS DR_{MMW} + BMP-2) and complex microgels (EPS DR_{MMW} + EPS
501 DRS_{LMW}/BMP-2) upon incubation in either 2 mM $CaCl_2$ or 180 mM $CaCl_2$ at 37°C for 23 or 27 days.
502 Release experiments were performed in duplicate for each condition and each time from two
503 independent encapsulation experiments.

504

505 The difference in BMP-2 release kinetics from complex microgels incubated at low and high
506 ionic strengths results most likely from the fact that at high salt concentration the screening of
507 charges decreased the binding strength between the positively charged BMP-2 and negatively
508 charged EPS DRS_{LMW}, favouring their dissociation. Similar results were reported for lysozyme
509 released from microparticles based on methacrylated hyaluronic acid and chondroitin sulfate at
510 different ionic strengths (Schuurmans *et al.*, 2018). By dissociating from the highly sulfated
511 derivative, soluble BMP-2 can then be quantified by ELISA assay. Indeed, tight complexation
512 of BMP-2 with EPS DRS_{LMW}, even at polysaccharide concentrations higher than 5 µg/mL,
513 prevented its appropriate quantification most likely through inhibition of binding between
514 BMP-2 and ELISA antibodies. Similar release profiles obtained in 180 mM $CaCl_2$ and DMEM

515 (Figure 4A and 4B) suggest that in DMEM, particularly rich in inorganic salts, BMP-2 also
516 dissociated from EPS DRS_{LMW}. It was further observed that only 14% to 20% of the initially
517 loaded growth factor was quantified, which could be due to incomplete BMP-2 dissociation
518 from EPS DRS_{LMW}. Similar results were also reported by Hettiaratchi *et al*. (2014), where less
519 than 20% of the BMP-2 initially loaded was released from heparin microparticles, suggesting
520 that the majority of the growth factor was retained inside the microparticles.
521 Although BMP-2 unbinding can appear inside microgels, it can also be thought that EPS
522 DRS_{LMW}/BMP-2 complex may diffuse outside the microgels and then dissociate or not,
523 depending on the ionic strength applied. To explore this hypothesis, the supernatants recovered
524 during BMP-2 release experiments at low and high ionic strengths were analyzed using
525 dynamic light scattering (DLS) and compared to control samples (BMP-2, EPS DRS_{LMW} and
526 EPS DRS_{LMW}/BMP-2 complex in water) (Figure 5). Two populations with hydrodynamic
527 diameters of 3.1 nm and 8.7 nm were measured for free BMP-2, which are consistent with the
528 size of the protein homodimer and the diameters of nanoparticles measured by AFM (Figure
529 3A). For EPS DRS_{LMW}, a predominant population of 28 nm was observed together with larger
530 aggregates of 295 nm in diameter, resulting most likely from further chain-chain associations.
531 When BMP-2 was complexed with EPS DRS_{LMW} in water, two populations were observed with
532 38 nm and 342 nm in diameter, corresponding to EPS DRS_{LMW}/BMP-2 complex and EPS
533 DRS_{LMW}, respectively. No peak of free BMP-2 was observed.
534 In the supernatant recovered during BMP-2 release from complex microgels at high ionic
535 strength (180 mM $CaCl_2$), the presence of soluble BMP-2 was noticed with the peak at 7.5 nm,
536 followed by a second peak at 24.4 nm corresponding to soluble EPS DRS_{LMW} and/or EPS
537 DRS_{LMW}/BMP-2 complex. The high amplitude of the first peak indicates the presence of free
538 BMP-2, suggesting dissociation of EPS DRS_{LMW}/BMP-2 complex. The low amplitude of the
539 second peak relative to EPS DRS_{LMW} alone and/or EPS DRS_{LMW}/BMP-2 complex suggests that

this dissociation may already take place inside microgels. In contrast, in the supernatant recovered during BMP-2 release from complex microgels at low ionic strength (2 mM $CaCl_2$), only one large peak at 18.2 nm was observed, which could be attributed to EPS DRS_{LMW}/BMP-2 complex and EPS DRS_{LMW}, while free BMP-2 was not observed. Therefore, it comes out that at low ionic strength EPS DRS_{LMW}/BMP-2 complexes diffuse outside the microgels and they do not dissociate at this low salt content. Diffusion of these complexes is facilitated by a looser microgel network formed in 2 mM $CaCl_2$. Hydrodynamic diameters of BMP-2 and EPS DRS_{LMW}/BMP-2 complexes measured by DLS in solution are in good agreement with AFM data presented on Figure 3.

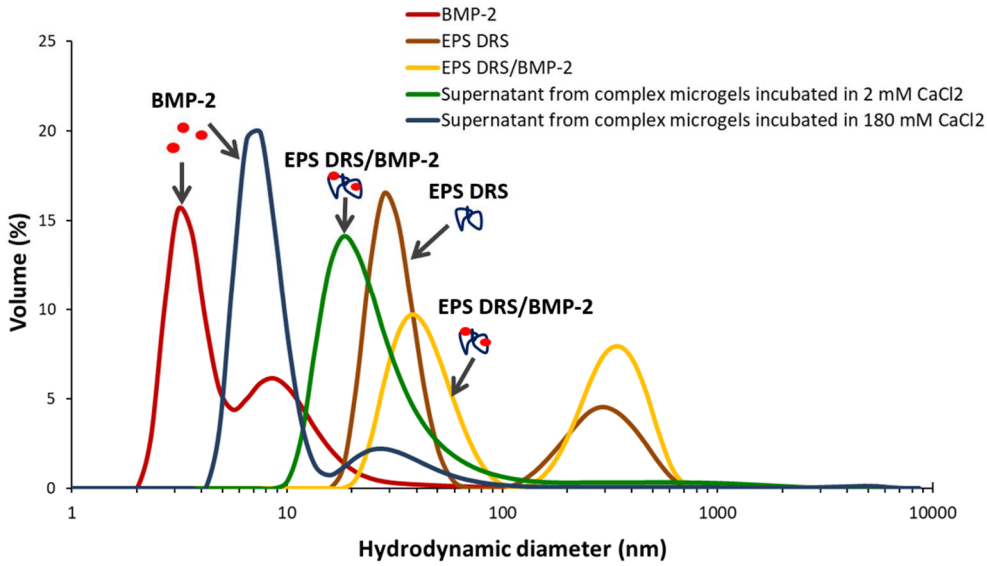

Figure 5. Hydrodynamic diameter of soluble BMP-2 (500 ng/mL), soluble EPS DRS_{LMW} (50 µg/mL) and EPS DRS_{LMW}/BMP-2 complexes in water as well as the supernatants recovered during the incubation of complex microgels in either 2 mM or 180 mM $CaCl_2$ for 48h.

3.4. BMP-2 bioactivity.

To assess the bioactivity of BMP-2 released from complex microgels in either DMEM or 2 mM $CaCl_2$, the phosphorylation of Smads 1,5,8 intracellular signaling proteins was investigated. Indeed, Smad 1 and the closely related Smads 5 and 8, specifically mediate BMP-2 responses, including the osteoblastic differentiation of precursor cell lines (Guicheux *et al.*, 2003;

Nishimura *et al.*, 1998; Yamamoto *et al.*, 1997). MC3T3-E1 cells were stimulated with the supernatants recovered after incubation of equilibrated complex microgels in either DMEM or 2 mM $CaCl_2$. It was clearly observed that BMP-2 maintained its biological activity, as evidenced by the activation of phosphorylation of Smads 1,5,8 (Figure 6). For BMP-2 released from complex microgels incubated in DMEM, a strong phosphorylation was observed over the entire first week and lower but still detectable activation after 14 and 21 days. Very similar results were observed in 2 mM $CaCl_2$ with a detectable activation measured up to 14 days. It appeared that BMP-2 complexation with EPS DRS_{LMW} did not preclude the appropriate binding of the BMP-2 to cell surface type I and II serine/threonine kinase receptors. The presence of this highly sulfated derivative seems essential to preserve the growth factor bioactivity for long-term period, as already shown for TGF-β1 (Merceron *et al.*, 2012; Zykwinska *et al.*, 2019b).

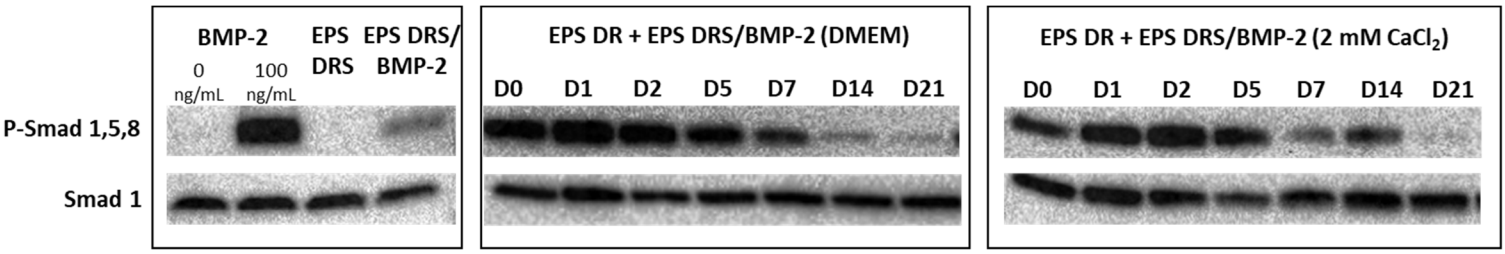

Figure 6. Bioactivity assessment of BMP-2 released from equilibrated complex microgels (EPS DR_{MMW} + EPS DRS_{LMW}/BMP-2) upon incubation in DMEM or 2 mM $CaCl_2$ at 37 °C for 21 days. Smad 1 and P-Smad 1,5,8 were detected by Western Blot using specific antibodies. Native BMP-2 (100 ng/mL), EPS DRS_{LMW} (50 µg/mL) and EPS DRS_{LMW}/BMP-2 (EPS DRS_{LMW} and BMP-2 final concentrations of 50 µg/mL and 500 ng/mL, respectively) were used as internal controls.

3.5. Effect of BMP-2 released from complex microgels on the *in vitro* osteogenic activity of hBM-MSC.

In order to address whether BMP-2 released from complex microgels may be able to stimulate the *in vitro* osteogenic activity of hBM-MSC, ALP activity and matrix mineralization were investigated. Indeed, ALP plays a key role in bone matrix mineralization by osteoblasts and is thus involved in bone formation (Hessle *et al.*, 2002). For this study, hBM-MSC were

physically separated from the BMP-2 loaded equilibrated complex microgels (EPS DR_{MMW} + EPS DRS_{LMW}/BMP-2) by a transwell membrane and cultured for 7 and 16 days (Figure 7A). In parallel, non-treated cells (NT), unloaded complex microgels (EPS DR_{MMW} + EPS DRS_{LMW}), unloaded complex microgels supplemented with soluble BMP-2 (100 ng/mL) (EPS DR_{MMW} + EPS DRS_{LMW} + sBMP-2) and soluble BMP-2 (100 ng/mL) were used as controls. Soluble BMP-2 was supplemented every three days. No statistical difference in ALP activity was found between BMP-2 loaded microgels, unloaded complex microgels and those supplemented with soluble BMP-2, and sBMP-2 (Figure 7B). The mineralization was effective in all four groups as underlined by the red alizarin coloration compared to NT (Figure 7C).

Although, BMP-2 loaded complex microgels induced ALP activity in similar manner than sBMP-2, the EPS-based microgels able to deliver bioactive BMP-2 to the surrounding microenvironment over several days present an undeniable advantage over exogeneous repeated supplementations of the growth factor (added every three days), clearly incompatible with *in vivo* treatments (Hettiaratchi *et al.*, 2020). Interestingly, unloaded complex microgels also displayed a positive impact on the ALP activity. This can result from the progressive swelling and dissolution of microgels, as observed during release experiments in DMEM, liberating both EPS DR_{MMW} and EPS DRS_{LMW}. Soluble EPS derivatives could then diffuse through transwell membrane and bind cell-secreted growth factors, including BMP-2, thus favoring cell signaling through growth factor/receptor interactions. No inhibitory effect related to the presence of a heparin-mimetic EPS DRS_{LMW} was noticed. In contrast, an inhibitory effect of heparin toward BMP-2-dependent mineralization has already been reported in osteoblast cells (Bramono *et al.*, 2012; Hausser & Brenner, 2004). Indeed, studies investigating the co-delivery of BMP-2 with soluble heparin have demonstrated either stimulatory or inhibitory effects on BMP-2 mediated osteogenesis (Kanzaki *et al.*, 2008, 2011; Ratanavaraporn & Tabata, 2012; Zhao *et al.*, 2006). Heparin was shown to be able to bind not only to BMP-2 but

604 also to its receptor, leading to a strong suppression of the expression of several genes well
605 known as essential factors in osteoblast differentiation (Runx2, osterix, ALP, osteocalcin) and
606 inhibition of the signaling pathways of Smads and p38 MAPK of MC3T3 (Kanzaki *et al*., 2008).
607 In contrast, in long-term cultures, heparin was shown to enhance the BMP-2 mediated
608 bioactivity by inhibiting binding to the growth factor of its antagonists (noggin, follistatin) and
609 inhibitory Smads 6, 7 (Kanzaki *et al*., 2011). It appears that depending on heparin molecular
610 weight, its sulfation pattern, its concentration and its presentation either in soluble or structured
611 form, opposite effects can be observed. Indeed, other studies on heparin structured in
612 microparticles for BMP-2 delivery have shown an increase in ALP activity compared to soluble
613 BMP-2 or co-delivered with soluble heparin (Hettiaratchi *et al*., 2014). Heparin-mimetic EPS
614 DRS_{LMW} used in our present study seems to exhibit stimulatory effects. Due to its lower
615 anticoagulant properties compared to low-molecular weight heparin or unfractionated heparin
616 (2.5 and 6.5 times, respectively) (Colliec-Jouault *et al*., 2001), this derivative may represent an
617 interesting alternative to heparin. Supplementary studies will be conducted to get further insight
618 into the osteogenic activity of BMP-2 loaded microgels. The impact of complex microgels on
619 osteogenic gene expression will be investigated in direct contact with cells to better match the
620 *in vivo* conditions. Finally, for an effective regenerative therapy, combination of these
621 microgels with an appropriate scaffold, e.g. injectable hydrogel will also be considered.

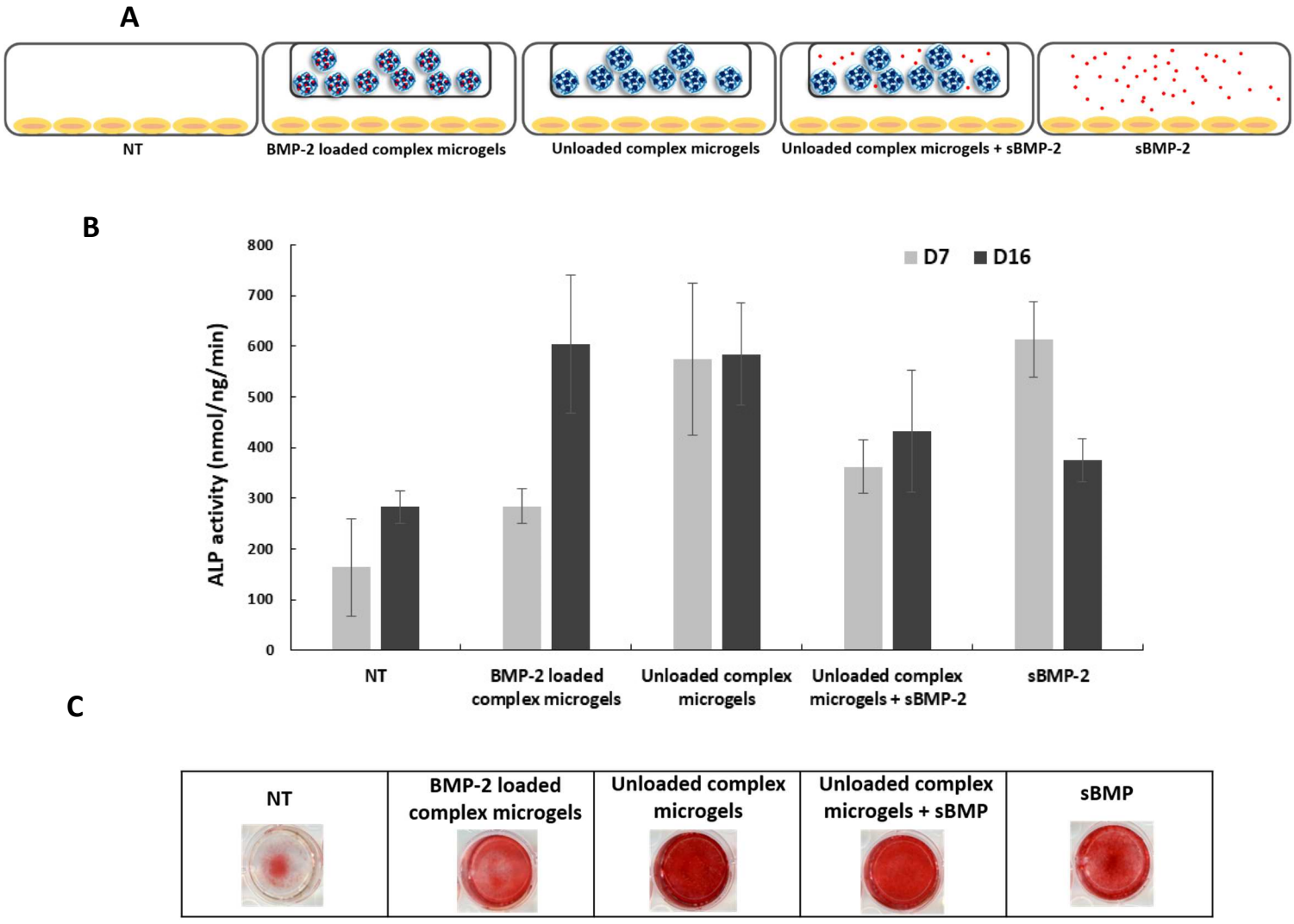

622

623 Figure 7. (A) Schematic representation of transwell experiment with the hBM-MSC incubated with
624 BMP-2 loaded complex microgels and control samples: no treatment (NT), unloaded complex
625 microgels, unloaded complex microgels supplemented with soluble BMP-2 (sBMP-2) and soluble
626 BMP-2 (sBMP-2). (B) ALP activity of hBM-MSC incubated with BMP-2 loaded complex microgels
627 and control samples. No significant differences were found between the different conditions. (C)
628 Mineralization of hBM-MSC pellets revealed by Alizarin red staining.

629

630

631

4. Conclusions

In the present study, a bacterial EPS displaying both GAG-mimetic and physical gelling properties was formulated into microgels for delivery of BMP-2, clinically used to promote bone formation. BMP-2 loading in single microgels based only on a slightly sulfated EPS DR_{MMW} did not provide a sustained release profile. In contrast, BMP-2 complexation with a highly sulfated low-molecular weight heparin-mimetic EPS DRS_{LMW} and its subsequent incorporation within microgels led to a progressive growth factor release. Release kinetics performed at low and high ionic strengths allowed to better understand the impact of salt concentration on growth factor release. At high ionic strength, such as in a cell culture medium, BMP-2 partly dissociated from EPS DRS_{LMW}, whereas at low ionic strength, BMP-2 was still tightly bound to the highly sulfated derivative. It was further shown that EPS DRS_{LMW}/BMP-2 complexes diffuse outside the microgels and that bound BMP-2 can also activate Smad signaling pathways. The presence of this highly sulfated heparin-mimetic derivative was essential to preserve the growth factor bioactivity for long-time period. BMP-2 loaded complex microgels were then explored for their pro-osteogenic properties by measuring both ALP activity and matrix mineralization induced by BMP-2 released from microgels during transwell experiments. Although BMP-2 loaded complex microgels induced ALP activity and induced matrix mineralization in similar manner to control samples, the EPS-based microgels able to deliver bioactive BMP-2 to the surrounding microenvironment over several days constitute an undeniable advantage over exogeneous repeated supplementations of the growth factor, clearly incompatible with therapeutic treatment. Taken together, the results obtained confirmed the initial hypothesis and emphasized that Infernan-based microgels constitute a promising platform for BMP-2 delivery. Further *in vitro* and *in vivo* studies will be performed to explore their bone healing potential.

Declarations of interest: The authors declare no conflict of interest.

Acknowledgments

The authors would like to thank Laetitia Marchand for monosaccharide analysis, Valérie Beaumal for DLS measurements and Mike Maillasson for SPR measurements. Nicolas Stéphan is acknowledged for his contribution in SEM imaging.

Financial support was provided by the French National Research Agency within the framework of the *FunCapsul* project (ANR-17-CE08-0001).

Author Contributions:

Perrine Gélébart: Methodology, Investigation, Formal analysis, Writing – Original Draft; **Stéphane Cuenot**: Conceptualization, Investigation, Validation, Writing – Review & Editing; **Corinne Sinquin**: Investigation, Formal analysis; **Boris Halgand**: Methodology, Investigation, Formal Analysis, Validation, Writing – Review & Editing; **Sophie Sourice**: Investigation, Formal analysis; **Catherine Le Visage**: Conceptualization, Writing – Review & Editing; **Jérôme Guicheux**: Conceptualization, Writing – Review & Editing; **Sylvia Colliec-Jouault**: Conceptualization, Writing – Review & Editing; **Agata Zykwinska**: Conceptualization, Methodology, Investigation, Validation, Funding acquisition, Writing – Original Draft.

680 **References**

681 Badri, A., Williams, A., Linhardt, R. J., & Koffas, M. A. G. (2018). The road to animal-free
682 glycosaminoglycan production: current efforts and bottlenecks. *Current Opinion in*
683 *Biotechnology*, *53*, 85-92.

684 Bessey, O. A., Lowry, O. H., & Brock, M. J. (1946). A method for the rapid determination of
685 alkaline phosphatase with five cubic millimeters of serum. *Journal of Biological Chemistry*,
686 *164*, 321–329.

687 Bhakta, G., Lim, Z. X. H., Rai, B., Lin, T., Hui, J. H., Prestwich, G. D., van Wijnen, A. J.,
688 Nurcombe, V., & Cool, S. M. (2013). The influence of collagen and hyaluronan matrices on
689 the delivery and bioactivity of bone morphogenetic protein-2 and ectopic bone formation. *Acta*
690 *Biomaterialia*, *9*, 9098-9106.

691 Bramono, D.S., Murali, S., Rai, B., Ling, L., Poh, W. T., Lim, Z. X., Stein, G. S., Nurcombe,
692 V., van Wijnen, A. J., & Cool, S. M. (2012). Bone marrow-derived heparan sulfate potentiates
693 the osteogenic activity of bone morphogenetic protein-2 (BMP-2). *Bone*, *50*, 954-964.

694 Caballero Aguilar, L. M., Silva, S. M., & Moulton, S. E. (2019). Growth factor delivery:
695 defining the next generation platforms for tissue engineering. *Journal of Controlled Release*,
696 *306*, 40-58.

697 Caetano-Lopes, J., Lopes, A., Rodrigues, A., Fernandes, D., Perpétuo, I. P., Monjardino, T.,
698 Lucas, R., Monteiro, J., Konttinen, Y., Canhao, H., & Fonseca, J. E. (2011). Upregulation of
699 inflammatory genes and downregulation of sclerostin gene expression are key elements in the
700 early phase of fragility fracture healing. *PLoS ONE*, *6*, e16947.

701 Chopin, N., Sinquin, C., Ratiskol, J., Zykwinska, A., Weiss, P., Cérantola, S., Le Bideau, J., &
702 Colliec-Jouault, S. (2015). A direct sulfation process of a marine polysaccharide in ionic liquid.
703 *BioMed Research International*, 508656.

704 Colliec-Jouault, S., Chevolot, L., Helley, D., Ratiskol, J., Bros, A., Sinquin, C., Roger, O., &
705 Fischer, A.-M. (2001). Characterization, chemical modifications and *in vitro* anticoagulant

properties of an exopolysaccharide produced by *Alteromonas infernus*. *Biochemical et Biophysica Acta*, 1528, 141–151.

DeAngelis, P. (2012). Glycosaminoglycan polysaccharide biosynthesis and production: today and tomorrow. *Applied Microbiology and Biotechnology*, *94*, 295-305.

Delbarre-Ladrat, C., Sinquin, C., Lebellenger, L., Zykwinska, A., & Colliec-Jouault, S. (2014). Exopolysaccharides produced by marine bacteria and their applications as glycosaminoglycan-like molecules. *Frontiers in Chemistry*, *2*, 1-15.

Ebara, S., & Nakayama, K. (2002). Mechanism for the action of Bone Morphogenetic Proteins and Regulation of their activity. *Spine*, *27*, 10-15.

Gandhi, N. S., & Mancera, R. L. (2008). The structure of glycosaminoglycans and their interactions with proteins. *Chemical Biology and Drug Design*, *72*, 455-482.

Gautschi, O.P., Frey, S.P., & Zellweger, R. (2007). Bone morphogenetic proteins in clinical applications. *ANZ Journal of Surgery*, *77*, 626-631.

Grivaud-Le Du, A., Zykwinska, A., Sinquin, C., Ratiskol, J., Weiss, P. Vinatier, C., Guicheux, J., Delbarre-Ladrat, C., & Colliec-Jouault, S. (2017). Purification of the exopolysacharied produced by Alteromonas infernus: identification of endotoxins and effective process to remove them. *Applied Microbiology and Biotechnology*, *101*, 6597-6606.

Guicheux, J., Lemonnier, J., Ghayor, C., Suzuki, A., Palmier, G., & Caverzasio, J. (2003). Activation of p38 mitogen-activated protein kinase and c-Jun-NH2-Terminal kinase by BMP-2 and their implication in the stimulation of osteoblastic cell differentiation. *Journal of Bone and Mineral Research*, *18*, 2060-2068.

Hausser, H.J., & Brenner, R.E. (2004). Low doses and high doses of heparin have different effects on osteoblast-like Saos-2 cells *in vitro*. *Journal of Cellular Biochemistry*, *91*, 1062-1073.

Hessle, L., Johnson, K. A., Anderson, H. C., Narisawa, S., Sali, A., Goding, J. W., Terkeltaub, R., & Millan, J. L. (2002). Tissue-nonspecific alkaline phosphatase and plasma cell membrane

731 glycoprotein-1 are central antagonistic regulators of bone mineralization. *Proceedings of the*
732 *National Academy of Sciences of the United States of America, 99*, 9445-9449.
733 Hettiaratchi, M. H., Miller, T., Temenoff, J. S., Guldberg, R. E., & McDevitt, T. C. (2014).
734 Heparin microparticle effects on presentation and bioactivity of bone morphogenetic protein-2.
735 *Biomaterials*, 35, 7228-7238.
736 Hettiaratchi, M. H., Krishnan, L., Rouse, T., Chou, C., McDevitt, T. C., & Guldberg, R. E.
737 (2020). Heparin-mediated delivery of bone morphogenetic protein-2 improves spatial
738 localization of bone regeneration. *Science Advances*, 6, 1-12.
739 Heymann, D., Ruiz-Velasco, C., Chesneau, J., Ratiskol, J., Sinquin, C., & Colliec-Jouault, S.
740 (2016). Anti-metastatic properties of a marine bacterial exopolysaccharide-based derivative
741 designed to mimic glycosaminoglycans. *Molecules*, *21*, 309.
742 Hogan, B. L. (1996). Bone morphogenetic proteins: Multifunctional regulators of vertebrate
743 development. *Genes and Development*, *10*, 1580-1594.
744 Jeon, O., Song, S. J., Yang, H. S., Bhang, S.-H., Kang, S.-W., Sung, M. A., Lee, J.H., & Kim,
745 B.-S. (2008). Long-term delivery enhances in vivo osteogenic efficacy of bone morphogenetic
746 protein-2 compared to shoty-term delivery. *Biochemical and Biophysical Research*
747 *Communications*, *369*, 774-780.
748 Kamerling, J. P., Gerwing, G. J., Vliegenthart, J. F., & Clamp, J. R. (1975). Characterization
749 by gas-liquid chromatography-mass spectrometry and proton-magnetic-resonance
750 spectroscopy of pertrimethylsilyl methyl glycosides obtained in the methanolysis of
751 glycoproteins and glycopeptides. Biochemical Journal, 151, 491-495.
752 Kanzaki, S., Takahashi, T., Kanno, T., Ariyoshi, W., Shinmyouzu, K., Tujisawa, T., &
753 Nishihara, T. (2008). Heparin inhibits BMP-2 osteogenic bioactivity by binding to both BMP-
754 2 and BMP receptor. *Journal of Cellular Physiology*, *216*, 844-850.
755 Kanzaki, S., Ariyoshi, W., Takahashi, T., Okinaga, T., Kaneuji, T., Mitsugi, S., Nakashima, K.,

Tsujisawa, T., & Nishihara, T. (2011). Dual effects of heparin on BMP-2-induced osteogenic activity in MC3T3-E1 cells. *Pharmacological Reports*, *63*, 1222–1230.

Kisiel, M., Klar, A. S., Ventura, M., Buijs, J., Mafina, M. K., Cool, S. M., & Hilborn, J. (2013). Complexation and sequestration of BMP-2 from an ECM mimetic hyaluronan gel for improved bone formation. *PLoS ONE*, *8*, 1-13.

Krishnan, L., Priddy, L. B., Esancy, C., Klosterhoff, B. S., Stevens, H. Y., Tran, L., & Guldberg, R. E. (2017). Delivery vehicle effects on bone regeneration and heterotopic ossification induced by high dose BMP-2. *Acta Biomaterialia*, *49*, 101-112.

Kusumoto, K., Bessho, K., Fujimura, K., Akioka, J., Ogawa, Y., & Iizuka, T. (1998). Prefabricated muscle flap including bone induced by recombinant human bone morphogenetic protein-2: An experimental study of ectopic osteoinduction in a rat latissimus dorsi muscle flap. *British Journal of Plastic Surgery*, *51*, 275-280.

Lavenus, S., Pilet, P., Guicheux, J., Weiss, P., Louarn, G., & Layrolle, P. (2011). Behaviour of mesenchymal stem cells, fibroblasts and osteoblasts on smooth surfaces. *Acta Biomaterialia*, *7*, 1525-1534.

Makshakova, O. N., Zykwinska, A., Cuenot, S., Colliec-Jouault, S., & Perez, S. (2022). Three-dimensional structures, dynamics and calcium-mediated interactions of the exopolysaccharide, Infernan, produced by the deep-sea hydrothermal bacterium *Alteromonas infernus*. *Carbohydrate Polymers*, *276*, 118732.

Marquis, M., Davy, J., Cathala, B., Fang, A., & Renard, D. (2015). Microfluidics assisted generation of innovative polysaccharide hydrogel microparticles. *Carbohydrate Polymers*, *116*, 189–199.

Merceron, C., Portron, S., Vignes-Colombeix, C., Rederstorff, E., Masson, M., Lesoeur, J., Sourice, S., Sinquin, C., Colliec-Jouault, S., Weiss, P., Vinatier, C., & Guicheux, J. (2012). Pharmacological modulation of human mesenchymal stem cell chondrogenesis by a chemically

781 oversulfated polysaccharide of marine origin: Potential application to cartilage regenerative
782 medicine. *Stem Cells*, *30*, 471-480.
783 Miller, T., Goude, M. C., McDevitt, T. C., & Temenoff, J. S. (2014). Molecular engineering of
784 glycosaminoglycan chemistry for biomolecule delivery. *Acta Biomaterialia*, *10*, 1705-1719.
785 Montreuil, J., Bouquelet, S., Debray, H., Fournet, B., Spik, G., & Strecker, G. (1986).
786 Glycoproteins. In Carbohydrate Analysis. A Practical Approach; Chaplin, M.F., Kennedy, J.F.,
787 Eds.; IRL Press: Oxford, UK, 143–204.
788 Moshaverinia, A., Xu, X., Chen, C., Akiyama, K., Snead, M. L., & Shi, S. (2013). Dental
789 mesenchymal stem cells encapsulated in an alginate hydrogel co-delivery microencapsulation
790 system for cartilage regeneration. *Acta Biomaterialia, 9*, 9343-9350.
791 Muir, J. M., Andrew, M., Hirsh, J., Weitz, J. I., Young, E., Deschamps, P., & Shaughnessy, S.
792 G. (1996). Histomorhometric analysis of the effects of standard heparin on trabecular bone *in*
793 *vivo*. *Blood*, *88*, 1314-1320.
794 Neovius, E., Lemberger, M., Docherty Skogh, A., Hilborn, J., & Engstrand, T. (2013). Alveolar
795 bone healing accompanied by severe swelling in cleft children treated with bone morphogenetic
796 protein-2 delivered by hydrogel. *Journal of Plastic, Reconstructive and Aesthetic Surgery*, *66*,
797 37-42.
798 Nishimura, R., Kato, Y., Chen, D., Harris, S. E., Mundy, G. R., & Yoneda, T. (1998). Smad5
799 and DPC4 are key molecules in mediating BMP-2-induced osteoblastic differentiation of the
800 pluripotent mesenchymal precursor cell line C2C12. *Journal of Biological Chemistry*, *273*,
801 1872–1879.
802 Okubo, Y., Bessho, K., Fujimura, K., Iizuka, T., & Miyatake, S. I. (2000). Osteoinduction by
803 bone morphogenetic protein-2 via adenoviral vector under transient immunosuppression.
804 *Biochemical and Biophysical Research Communications*, *267*, 382–387.
805 Poynton, A. R., & Lane, J. M. (2002). Safety profile for the clinical use of bone morphogenetic

proteins in the spine. *Spine*, *27*, 40-48.

Raguénès, G., Peres, A., Ruimy, R., Pignet, P., Christen, R., Loaec, M., Rougeaux, H., Barbier, G., & Guezennec, J. G. (1997). *Alteromonas infernus* sp. Nov., a new polysaccharide producing bacterium isolated from a deep-sea hydrothermal vent. *Journal of Applied Microbiology*, *82*, 422-430.

Ratanavaraporn, J., & Tabata, Y. (2012). Enhanced osteogenic activity of bone morphogenetic protein-2 by 2-O-desulfated heparin. *Acta Biomaterialia*, *8*, 173-182.

Rederstorff, E., Rethore, G., Weiss, P., Sourice, S., Beck-Cormier, S., Mathieu, E., Maillasson, M., Jacques, Y., Colliec-Jouault, S., Fellah, B. H., Guicheux, J., & Vinatier, C. (2017). Enriching a cellulose hydrogel with a biologically active marine exopolysaccharide for cell-based cartilage engineering. *Journal of Tissue Engineering and Regenerative Medicine*, *11*, 1152-1164.

Roger, O., Kervarec, N., Ratiskol, J., Colliec-Jouault, S. & Chevolot, L. (2004). Structural studies of the main exopolysaccharide produced by the deep-sea bacterium *Alteromonas infernus. Carbohydrate Research*, *339*, 2371-2380.

Scheufler, C., Sebald, W., & Hülsmeyer, M. (1999). Crystal structure of human Bone Morphogenetic Protein-2 at 2.7 Å resolution. Journal of Molecular Biology, 287, 103-115.

Schuurmans, C.C.L., Abbadessa, A., Bengtson, M.A., Pletikapic, G., Eral, H. B., Koenderink, G., Masereeuw, R., Hennick, W. E., & Vermonden, T. (2018). Complex coacervation-based loading and tunable release of a cationic protein from monodisperse glycosaminoglycan microgels. *Soft Matter*, *14*, 6327–6341.

Shields, L. B. E., Raque, G. H., Glassman, S. D., Campbell, M., Vitaz, T., Harpring, J., & Shields, C. B. (2006). Adverse effects associated with high-dose recombinant human bone morphogenetic protein-2 use in anterior cervical spine fusion. *Spine*, *31*, 542–547.

Subbiah, R., & Guldberg, R. E. (2019). Materials science and design principles of growth factor

delivery systems in tissue engineering and regenerative medicine, *Advanced Healtcare Materials*, *8*, 1801000.

Takada, T., Katagiri, T., Ifuku, M., Morimura, N., Kobayashi, M., Hasegawa, K., Ogamo, A., & Kamijo, R. (2003). Sulfated polysaccharides enhance the biological activities of Bone Morphogenetic Proteins. *Journal of Biological Chemistry*, *278*, 43229-43235.

Tellier, L.E., Miller, T., McDevitt, T. C., & Temenoff, J. S. (2015). Hydrolysis and sulfation pattern effects on release of bioactive bone morphogenetic protein-2 from heparin-based microparticles. *Journal of Material Chemistry B*, *40*, 8001-8009.

Wolinsky-Friedland, M. (1995). Drug-induced metabolic bone disease. *Endocrinology and Metabolism Clinics of North America*, *24*, 395–420.

Yamamoto, N., Akiyama, S., Katagiri, T., Namiki, M., Kurokawa, T., & Suda, T. (1997). Smad1 and smad5 act downstream of intracellular signaling of BMP-2 that inhibits myogenic differentiation and induces osteoblast differentiation in C2C12 myoblasts. *Biochemical and Biophysical Research Communications*, *238*, 574–580.

Zhang, H., Tumarkin, E., Sullan,, R.M.A., Walker, G. C., & Kumacheva, E. (2007). Exploring microfluidic routes to microgels of biological polymers. *Macromolecular Rapid Communications*, *28*, 527–538.

Zhao, B., Katagiri, T., Toyoda, H., Takada, T., Yanai, T., Fukuda, T., Chung, U., Koike, T., Takaoka, K., & Kamijo, R. (2006). Heparin potentiates the in vivo ectopic bone formation induced by bone morphogenetic protein-2. *Journal of Biological Chemistry*, *281*, 23246-23253.

Zykwinska, A., Marchand, L., Bonnetot, S., Sinquin, C., Colliec-Jouault, S., & Delbarre-Ladrat, C. (2019a). Deep-sea hydrothermal vent bacteria as a source of glycosaminoglycan-mimetic exopolysaccharides. *Molecules*, *24*, 1–11.

Zykwinska, A., Marquis, M., Sinquin, C., Cuenot, S., & Colliec-Jouault, S. (2016). Assembly of HE800 exopolysaccharide produced by a deep-sea hydrothermal bacterium into microgels

for protein delivery applications. *Carbohydrate Polymers*, *142*, 213–221.

Zykwinska, A., Marquis, M., Godin, M., Marchand, L., Sinquin, C., Garnier, C., Jonchère, C., Chédeville, C., Le Visage, C., Guicheux, J., Colliec-Jouault, S., & Cuenot, S. (2019b). Microcarriers based on glycosaminoglycan-like marine exopolysaccharide for TGF-β1 long-term protection. *Marine Drugs*, *17*, 1–15.

Zykwinska, A., Marquis, M., Sinquin, C., Marchand, L., Colliec-Jouault, S., & Cuenot, S. (2018). Investigation of interactions between the marine GY785 exopolysaccharide and transforming growth factor-β1 by atomic force microscopy. *Carbohydrate Polymers*, *202*, 56–63.

Graphical abstract